Lab on a Chip

PAPER

View Article Online
View Journal

Cite this: DOI: 10.1039/d3lc00313b

A microfluidic mechano-chemostat for tissues and organisms reveals that confined growth is accompanied with increased macromolecular crowding†

Zacchari Ben Meriem,‡[a] Tiphaine Mateo,‡[a] Julien Faccini,[a] Céline Denais,[a] Romane Dusfour-Castan,[b] Catherine Guynet,[b] Tatiana Merle,[c] Magali Suzanne,[c] Mickaël Di-Luoffo,[d] Julie Guillermet-Guibert,[de] Baptiste Alric,[a] Sylvain Landiech,[a] Laurent Malaquin,[a] Fabien Mesnilgrente,[a] Adrian Laborde,[a] Laurent Mazenq,[a] Rémi Courson[f] and Morgan Delarue *[a]

Conventional culture conditions are oftentimes insufficient to study tissues, organisms, or 3D multicellular assemblies. They lack both dynamic chemical and mechanical control over the microenvironment. While specific microfluidic devices have been developed to address chemical control, they often do not allow the control of compressive forces emerging when cells proliferate in a confined environment. Here, we present a generic microfluidic device to control both chemical and mechanical compressive forces. This device relies on the use of sliding elements consisting of microfabricated rods that can be inserted inside a microfluidic device. Sliding elements enable the creation of reconfigurable closed culture chambers for the study of whole organisms or model micro-tissues. By confining the micro-tissues, we studied the biophysical impact of growth-induced pressure and showed that this mechanical stress is associated with an increase in macromolecular crowding, shedding light on this understudied type of mechanical stress. Our mechano-chemostat allows the long-term culture of biological samples and can be used to study both the impact of specific conditions as well as the consequences of mechanical compression.

Received 11th April 2023,
Accepted 9th September 2023

DOI: 10.1039/d3lc00313b

rsc.li/loc

Introduction

Cells in tissues and organisms, or during development, are constantly subjected to dynamic chemical and mechanical cues. Imposing dynamic chemical conditions on 3D cellular assemblies is a technical challenge that requires the use of complex microfluidic devices.[1–4] However, despite the large parallelization enabled by some of these devices, they do not necessarily allow easy dynamic control, and very few enable the establishment of chemical spatial gradients[5,6] which are essential to study 3D chemotaxis or drug screening. Mechanically, and apart from devices allowing control of shear or tensile stresses,[7,8] the appropriate 3D mechanical conditions to study the effect of spatial confinement and compressive stresses are lacking.

Compressive stresses can either be dynamic, such as peristalsis during digestion or the compression of articular cartilage during motion,[9] or self-inflicted in the case of spatially constrained growth[10] – the so-called growth-induced pressure. Indeed, compressive stress naturally arises when cells proliferate in a confined space, like solid tumors growing within an organ.[11] Compressive stresses can be deleterious for tumor treatment since they can clamp blood vessels,[12] modulate cell proliferation,[13–15] and even participate in a mechanical form of drug resistance.[15] In contrast with tensile and shear stresses,[16–21] very little is known about the sensing of mechanical pressure.

Growth-induced pressure is notoriously hard to study. Current methods to impose spatial confinement either rely on open-facing devices[22] or spheroid embedding in a hydrogel.[13–15] While hydrogel embedding displays natural limitations in terms of the type and size of the studied

[a] LAAS-CNRS, Université de Toulouse, CNRS, Toulouse, France. E-mail: morgan.delarue@laas.fr
[b] Laboratoire de Microbiologie et de Génétique Moléculaires, Centre de Biologie Intégrative (CBI), CNRS, Université de Toulouse, F-31000, Toulouse, France
[c] Molecular, Cellular and Developmental Biology unit (MCD), Centre de Biologie Intégrative (CBI), Université de Toulouse, CNRS, UPS, France
[d] INSERM U1037, CRCT, Université de Toulouse, F-31037 Toulouse, France
[e] Laboratoire d'Excellence TouCAN, F-31037 Toulouse, France
[f] Ifremer, RDT, F-29280 Plouzané, France

† Electronic supplementary information (ESI) available. See DOI: https://doi.org/10.1039/d3lc00313b

‡ These authors contributed equally.

sample as well as its retrieval for further biological characterization and the dynamic control of the culture conditions, open-facing devices do not fully confine tissues which can grow in the third dimension, leading to a poor buildup of growth-induced pressure in the Pa range,[23] far from the typical kPa range of pressure measured during hydrogel embedding.[15]

In general, the culture of organisms inside microfluidic devices remains difficult to do, even though microfluidic systems can offer much tighter control than classical culture. In this paper, we present a generic microfluidic device that takes advantage of an innovative technology called sliding elements. Sliding elements are microfabricated rods that can be inserted inside a microfluidic device. Using this technology, we created reconfigurable confining culture chambers which could be loaded with biological objects such as spheroids in order to study the impact of growth-induced pressure. This device permits great chemical and mechanical control, real-time imaging, and the possibility to recover the sample. Novel pressure sensors have been developed to measure growth-induced pressure. We demonstrated that our device was fitted for the controlled culture of multicellular spheroids, and showed that growth-induced pressure was associated with increased macromolecular crowding, thus

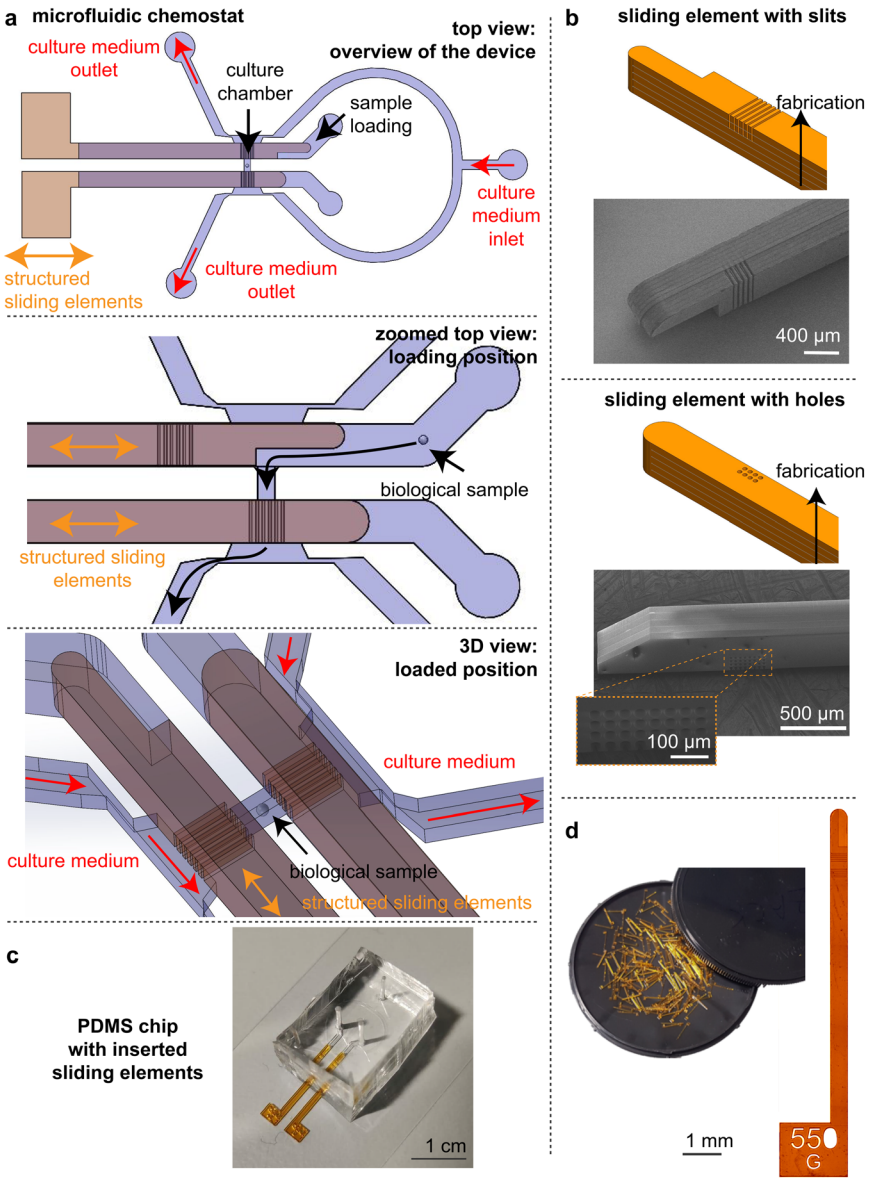

Fig. 1 Design of the microfluidic chemostat. a. The microfluidic chemostat is composed of a culture chamber that is closed on both sides by structured sliding elements. These elements enable to load the chamber and feed the sample thanks to channels on both sides. b. Standard photolithography is used on dry films to structure in 3D the element. Depending on the direction of construction, we can either construct slits or holes. Scanning electron images of the sliding elements are presented. c. Picture of the microfluidic device with the sliding elements inserted. d. The sliding elements are centimetric in length and structured at the tens of micrometer resolution. They are fabricated by the hundreds and can be inserted in a PDMS chip.

shedding light on a novel biophysical regulation of confined growth in mammalian cells. Prospectively, we showed that our device can be used for the culture of other organisms, such as the nematode *C. elegans* or imaginal discs of the *D. melanogaster*.

Results

Sliding elements to create a microfluidic chemostat for biological samples

The realization of a microfluidic chemostat resides in our ability to load a sample at a given position and define the chemical environment around it (Fig. 1a). Valves could be used to trap a sample, but the feeding remains difficult. Solutions relying on one-way valves have been developed for microbes,[10,24] but are not directly amenable to larger and deformable samples. To overcome this difficulty, we underwent a key technological development: sliding elements, tiny 3D-structured rods which can be inserted inside a microfluidic system to bring specific functions of interest.[25] By coupling standard photolithography and the use of dry film photoresists, we created well-defined and transparent sliding elements with cylindrical holes or slits depending on the direction of fabrication (Fig. 1b). They were centimetric in length and squared in the other dimensions with a cross size of 500 μm, making them easy to manipulate and slide into a designated channel (Fig. 1c). We created them by the hundreds in one batch (Fig. 1d, inset).

Culture chambers were molded in polydimethylsiloxane (PDMS) from molds created using multi-level photolithography, the first one defining the height of the culture chamber, while the second one delineated the channel into which the sliding element would be inserted (Fig. 1c). The height of this channel had to be optimized to ensure tight sealing and avoid medium leakage from one compartment to the next. We find that the channel with the sliding element did not leak for fluid pressure below 200 kPa, which was above the typical maximum 50 kPa pressure needed in our experiments to culture cells (Fig. S1†). The leakage occurred along the sliding element, probably because of slight misalignment during the fabrication process, and even at 200 kPa, no liquid went through the main channel. This tight sealing was essential to enable perfect control over the chemical environment. Notably, we showed that we could instantaneously change the chemical conditions in the chamber (Fig. S2†). We could have a fresh medium with constant chemical conditions circulating or allow a fixed volume of medium to cyclically re-circulate in the chamber to either decrease waste or perform specific enrichment experiments.

Steady culture of multicellular spheroids

The chemostat could be smoothly loaded with various biological objects. Sliding one element down opens one side of the chamber so that by adjusting the inlet flow, we could control the position of a multicellular spheroid inside the chamber, pushing it to the end, or retrieving it. We showed that spheroids can be cultured in the device for days (Fig. 2a and ESI† Video S1), with no significant differences in growth measured inside the device in comparison with classical culture in well plates (Fig. 2b). Each replicate in Fig. 2b is made with a different PDMS chip, a different set of sliding elements, and a different spheroid, demonstrating the robustness and reproducibility of the experiments. Of note,

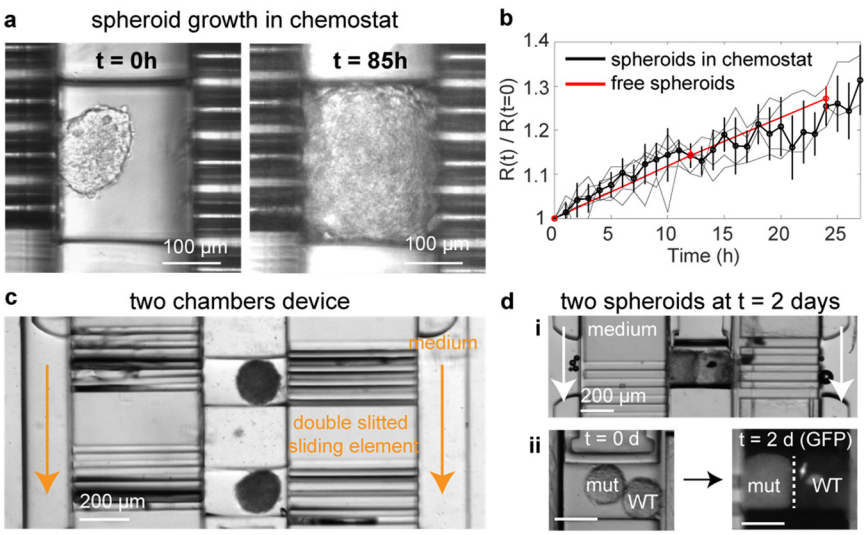

Fig. 2 Culture of multicellular spheroids in the microfluidic chemostat. a. Multicellular spheroids can be loaded in the chemostat. They can grow until they fill the chamber. b. Growth curves of spheroids in the chemostat (6 independent replicates – unique spheroid, unique PDMS chip and unique set of sliding elements – in light black) and in classical round bottom well plates (mean ± SEM). Thick lines represent median ± standard deviation. c. We designed devices with two parallel chambers where different samples can be loaded and cultured. d. Two different spheroids can be loaded and cultured in the same chamber (i). They grow until the chamber is filled (ii).

we could parallelize the chambers, different spheroids could be loaded in different chambers (Fig. 2c), to increase throughput or parallelize experiments. Interestingly, we can also load two different samples in the same chamber (Fig. 2di and ii). This unique feature, which cannot be done in open-facing devices or in hydrogels, is of particular interest to study interactions (mechanical and chemical) between different samples, and perform mechanical competition for space.[26]

Confined proliferation and growth-induced pressure

Fully confining cells would require to decrease the size of holes or slits in the sliding elements to avoid cells escaping from them. Cells are indeed able to migrate and deform through constrictions as small as 5 μm,[27] which was a resolution not reachable during sliding element fabrication. To overcome this issue, we designed a three-layer system with a culture chamber connected on its side to much smaller

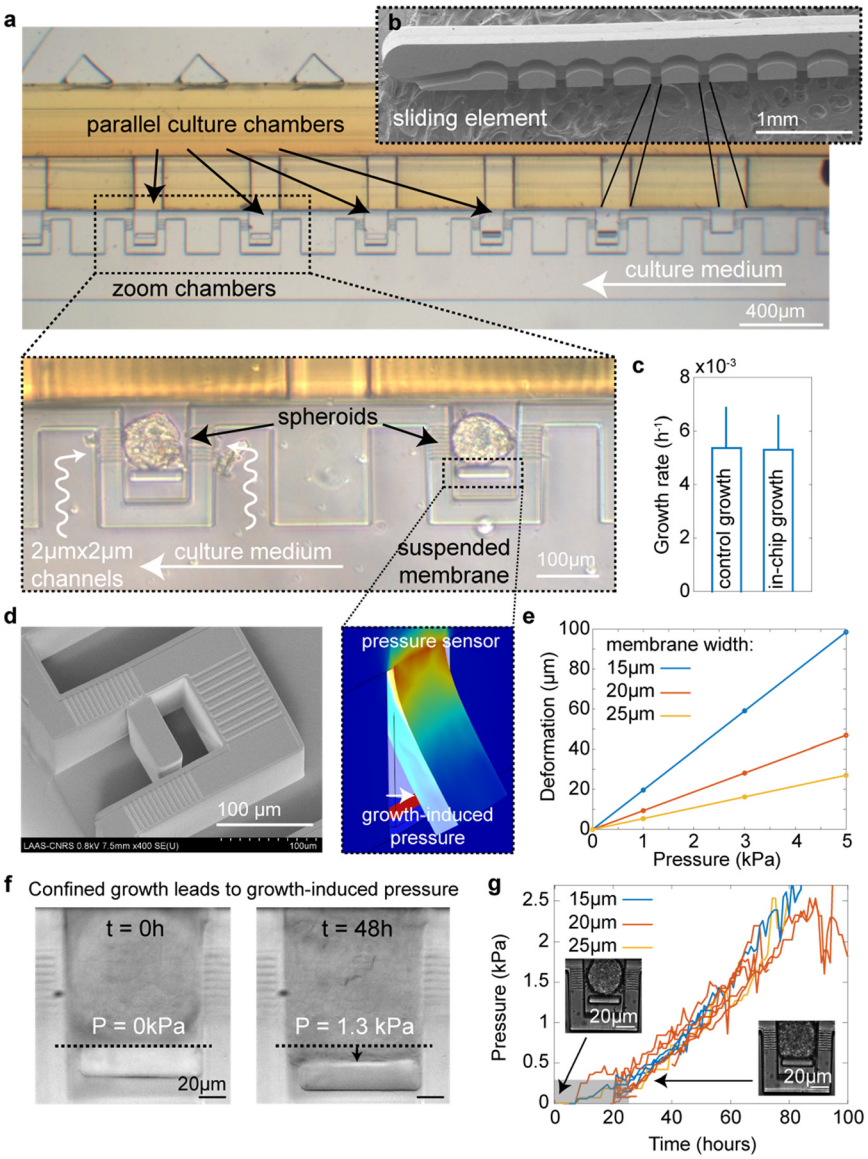

Fig. 3 Confined growth of multicellular spheroids and pressure sensor. a. The design can be parallelized and built on three levels to create multiple closed culture chambers. b. The sliding element is structured in such a way as to allow the loading and closing of the chambers. c. The growth rate of multicellular spheroids before confinement is similar to that of free spheroids (median ± standard deviation, N = 4 independent experiments). d. Scanning electron microscopy image of the chamber containing the suspended membrane. Image of a finite element simulation showing its deformation when a fixed pressure is applied. e. Deformation of the membrane with applied pressure as a function of membrane width. f. Confined growth leads to growth-induced pressure measured by the deformation of the suspended membrane. g. Pressure is independent of the width of the suspended membrane. After a slow increase which corresponds to a change of spherical shape to a cube, pressure increases roughly linearly for hours. The grayed area corresponds to the time points for which pressure is underestimated owing to the aggregate not fully contacting the surface. 10 spheroids over 4 independent experiments.

channels (2 μm × 2 μm in cross-section) which fully blocked the spheroid (Fig. 3a). We adapted the design of the sliding element to load and close these chambers (Fig. 3b and ESI† Video S2), and observed that spheroids grew fully confined in this geometry (ESI† Video S3), without invading the side channels. Normal growth of the spheroid was measured before being spatially confined (Fig. 3c), suggesting optimal feeding.

Confined growth eventually leads to the buildup of growth-induced pressure.[28] Evaluating growth-induced pressure often relies on the measurement of the surrounding deformation,[13,15,29] or the deformation of exogenous sensors such as hydrogel beads.[30,31] Alternatively, micropillars have been widely used to measure kPa stresses exerted by moving cells[32] or growing spheroids in open-facing devices,[22,23] due to their high deformation when sufficiently thin. We adapted this technology to design a thin suspended membrane to measure growth-induced pressure (Fig. 3d). We performed finite element simulations to tune its dimensions to be sensitive to the kPa range[15] (Fig. 3e). We observed that at similar dimensions, a fully attached membrane was much less deformable than one attached only at the top (Fig. S3†). In order to calibrate the mechanical properties of the PDMS, a crucial parameter to perfectly infer the pressure exerted onto the membrane from its deformation, we designed a fully attached membrane and measured its deformation with a fixed pressure. The deformation as a function of pressure was used to determine the mechanical properties of the PDMS of the chip thanks to finite element simulations, allowing the proper calibration of the mechanical properties (Fig. S4†). Of note, we could also use this membrane to instantaneously compress a trapped multicellular spheroid or a collagen gel (Fig. S5†).

We observed that the confined proliferation of a spheroid led to the progressive build-up of growth-induced pressure over the kPa range for several days (Fig. 3f and ESI† Video S3). The dynamics did not depend on the width of the suspended membrane (Fig. 3g) and was very comparable to what would be expected for these cells using a standard hydrogel embedding (Fig. S6†). This indicated that cells were similarly fed in both conditions and that growth-induced pressure development did not depend on the type of spatial confinement. Note that we needed to apply a correction factor when the spheroid did not fully contact the membrane (Fig. S7†). Because this factor could not be easily determined with our imaging conditions, for pressures below 250 Pa, the pressure was underestimated – these points were grayed on the figure. Interestingly, we observed that during the first 24 h, the spheroid deformed into a cuboid, while developing a growth-induced pressure of ~300 Pa. We showed (see Methods) that this information can be used to quantify the surface tension of a spheroid, which in this case is in the range of 1.5 mN m^{-1}, consistent with measurements in other cell types done with classical micropipette aspiration.[33]

Importantly, the chambers can be re-opened to allow a non-chemical relaxation of the mechanical stress. The samples can be retrieved for further biological analysis, even after having been under mechanical pressure (Fig. S8†). Note that the tissue remained cuboidal after being retrieved from the chamber. This essential point was often a bottleneck in microfluidics, and relaxing mechanical stress in hydrogel embedding systems requires the use of chemicals,[34] both of which the use of sliding elements easily overcame.

Growth-induced pressure increased intracellular crowding and decreased proliferation

We sought to investigate the cellular response to growth-induced pressure. We measured cellular densification within the compressed tissue, suggesting that single cells were more compressed under confined growth (Fig. S9†). Taking advantage of the fact that microfluidics allows high-resolution imaging, we used the FUCCI cell-cycle marker (Fig. 4a) and measured a progressive accumulation of G1 cells as growth-induced pressure increased (Fig. 4b). This result was consistent with former findings showing an association between growth-induced pressure and physiological changes, and notably a decrease in cell proliferation.[13,15,29,34,35]

An elusive question in mechano-biology relates to how growth-induced pressure is integrated and, especially which cellular biophysical properties are modified. It has recently been shown in the budding yeast *Saccharomyces cerevisiae* that growth-induced pressure is accompanied by an increase in intracellular crowding,[28] which relates to the high packing fraction of macromolecules in cells.[36] Genetically-encoded multimeric nanoparticles (GEMs) can be imaged at the single cell level in order to infer intracellular crowding through single particle tracking[37] (Fig. 4c). Using GEMs, we sought to investigate how intracellular crowding was modified in mammalian cells during the buildup of growth-induced pressure. We found that the mean diffusion coefficient was decreasing with increased growth-induced pressure (Fig. 4d), suggesting that, similarly to *S. cerevisiae*, intracellular crowding increased during confined proliferation and with the buildup of growth-induced pressure. Note that the control condition of unconfined growth in the chip corresponded to partial confinement of the spheroid: it was only allowed to grow in one direction, similar to what happens in an open-facing device.[22] In this case, we noticed no change in the diffusion of the nanoparticles, further illustrating the difference in the impact of full confinement in contrast to partial one.

Conclusions

We reported in this article a generic microfluidic device allowing the controlled confined culture of multicellular spheroids. Its operation relied on a key and novel technological development, sliding elements, which could be inserted inside a PDMS device to create reconfigurable culture chambers. Sliding elements could be produced by the hundreds, and allowed exquisite resolution thanks to the

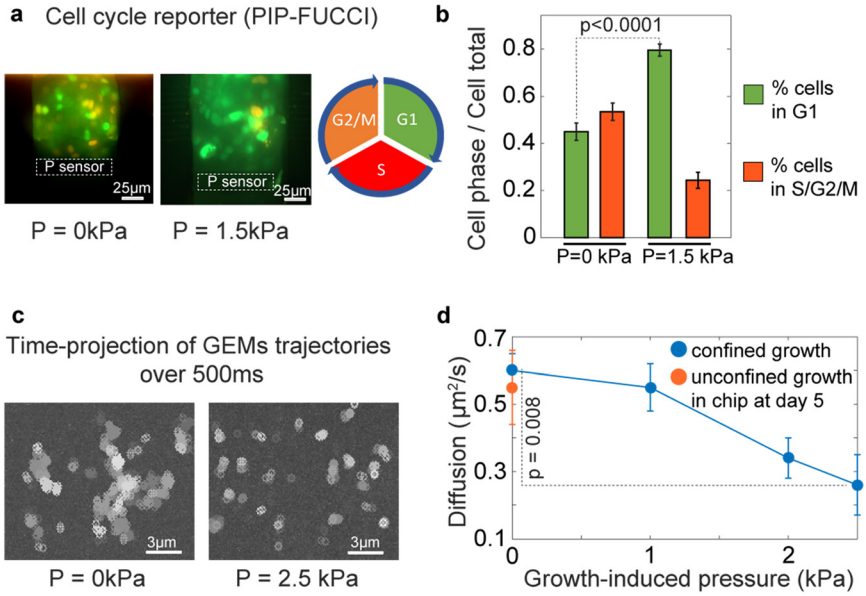

Fig. 4 Confined growth leads to growth-induced pressure which impacts cell proliferation and intracellular crowding. a. FUCCI cell cycle reporter to fluorescently label cell cycle phases. Representative images of FUCCI-labeled cells in the device for different growth-induced pressure values. b. Cells accumulate in G1 as growth-induced pressure builds up. 6 spheroids over 4 independent experiments were analyzed. c. Time projection of GEMs nanoparticles trajectories shows that particles are less diffusive under growth-induced pressure. d. Diffusion progressively decreases as growth-induced pressure increases. $N \geq 10$ cells for each point coming from 6 spheroids over 3 independent experiments. For all points, we computed the mean ± standard error of the mean.

power of photolithography. In particular, they could be structured by channels or holes, which allowed us to close a culture chamber while retaining the ability to feed the sample loaded in this chamber, something that a classical valve could not do.

The full confinement of a spheroid allows the study of growth-induced pressure. While hydrogel embedding can appear as an easier alternative, they do not offer the control that microfluidics permits. In particular, retrieving the spheroid after the experiment or relaxing growth-induced pressure without potential chemical stress is a challenge. Moreover, our device uniquely allows us to study the direct mechanical interaction of multicellular spheroids[26] (Fig. 2d), which is not possible through hydrogel embedding. Finally, open-facing systems do not fully confine spheroids, which leads to a poor buildup of mechanical stress and makes the study of this key mechanical stress impossible.

The confined growth of multicellular spheroids led to the buildup of growth-induced pressure, which has a number of physiological consequences. We developed a novel mechanical sensor to measure mechanical pressure and demonstrated that spheroids in our device could develop growth-induced pressure. In particular, their transition from a spheroid to a cuboid shape allows the estimation of the tissue surface tension independently of other viscoelastic and poromechanics parameters. How growth-induced pressure is integrated and impacts cells are mostly unknown, in contrast to other types of mechanical stresses, such as tensile[16] or shear.[21] We showed that while cell proliferation was decreased, as previously reported,[15,34] intracellular crowding increased concomitantly with growth-induced pressure in mammalian cells, yielding a novel biological insight on the mechanisms that can be associated with the integration of growth-induced pressure. To our knowledge, this is the first demonstration in mammalian cells that growth-induced pressure is associated with increased crowding. This was previously shown in the budding yeast *S. cerevisiae*,[28] raising the question of the universality of this phenomenon.

Our device could be used for the culture of other organisms. The system could be loaded with different organisms the same way a spheroid was (Fig. 1 and 2). Prospectively, we demonstrated that both moving nematodes and imaginal discs could be cultured in the device. We showed that we could harmlessly load the nematode *C. elegans* and culture it for at least 10 h (Fig. 5a and ESI† Video S4). The worm remained trapped in the culture chamber, permitting its imaging under fixed chemical conditions. Additionally, we validated the loading and culture of imaginal discs, such as the *Drosophila melanogaster* leg (Fig. 5b, ESI† Video S5). The smooth manipulation and culture in the chamber allowed us to monitor its development for 20 h which was similar in the chemostat compared to classical culture conditions.[38] The steady chemical environment, produced using syringe pumps, allowed long culture times, typically hard to reach with classic culture conditions where culture medium volume is fixed.[39]

In conclusion, we developed single-cast microfluidic devices for the long-term culture of biological samples and their confinement. These devices are parallelable to increase

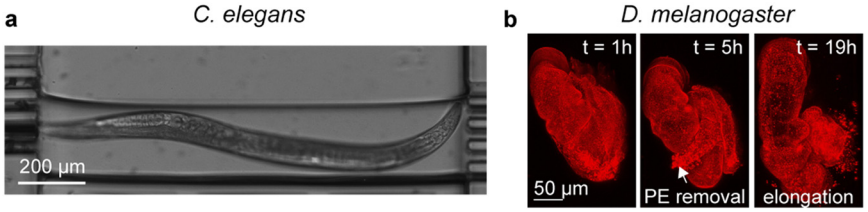

Fig. 5 Culture of moving organism or imaginal discs. a. Moving samples such as the nematode *C. elegans* can be cultured in the device. $N = 5$ independent experiments. Worms have been culture for 10 hours. b. Imaginal discs such as a drosophila leg can be loaded, and display normal development in the microfluidic chemostat, as seen by the timing of PE removal and leg elongation. $N = 3$ independent experiments. The wing has been cultured for 20 h.

throughput, and can be used to study both the impact of specific chemical conditions and the consequences of mechanical compression as well as mechanically characterizing a multicellular spheroid. Compressive stress is still poorly understood owing to the lack of tools available to researchers. Our device offers an elegant solution to its study.

Material and methods

Device microfabrication

The chemostat is made from a two-layer silicon mold. The high-throughput tumor-on-chip is made from a three-layer silicon mold. For the high-throughput device, we have an initial layer allowing to create the culture channels. This layer is not present in the chemostat where feeding is ensured through the sliding element. All layers are created using dry film technology.

In order to generate channels alimentation which are characterized by a very tiny section of 2 × 2 µm, an initial layer made of a mix of two SU8 photoresist (SU8-6000.5 and SU8 60005, ratio 1:1) is spin-coated (speed: 2500 rpm, acceleration: 3000 rpm s^{-1}, time: 30 s) with the spin coater Suss Microtec, on a silicon wafer substrate and cured (2 min at 100 °C). The photoresist is exposed with the MA6 Gen4 machine (I-line 37% at 300 mJ cm^{-2}) with the first mask design and cured (100 °C for 2 min) by following standard photolithography processes. To create the second layer defining the culture chamber, a 100 µm dry film is laminated above the mold (pressure: 2.5 bars, speed: 0.5 m min^{-1}, temperature: 100 °C for all lamination), and is exposed using a second mask (I-line 37% at 240 mJ cm^{-2}) and cured (100 °C during 6 min). The last layer is created from a stack lamination of four 100 µm dry-film sheets in order to create the 500 µm channel used to insert the sliding element. Then, exposure is performed (I-line 37% at 2000 mJ cm^{-2}) and the mold is cured (PEB of 100 °C during 20 min). During exposure steps, particular caution is necessary to align each level with the previous one.

A chemical development in SU8-developper bath is done at the end of the process in order to reveal the channels. Afterward, a hard-bake is performed to reinforce the mold's mechanical resistance through time. A perfluorodecyltrichlorosilane (FDTS) self-assembled monolayer is grafted onto the surface to prevent polydimethylsiloxane (PDMS) adhesion.

PDMS is cast onto the mold and cured at 65 °C overnight. The chip is initially sealed with a thin 50 µm PDMS layer by plasma activating the two surfaces with oxygen plasma (0.2 mBar, 0.7 sccm, 25 s) with the Diener Electronics machine in order to have the same material onto the culture chamber walls. Finally, the whole chip is sealed on a glass slide using the same parameters for plasma O2 activation.

Once made, the mold surface is controlled by Scanning Electron Microscopy (MEB Hitachi S-4800). Tension and current are respectively set at 0.6 kV and 8 µA. To correct astigmatism, magnification is set at ×3000. The image definition is about 1200 × 900 px.

Sliding element fabrication

The sliding element is made of two different levels (300 µm and 200 µm), using dry film technology, which allows additive fabrication. Each level required stack lamination of 100 µm dry film sheet and is laminated using the same parameters as the mold fabrication. Starting from a silicon wafer substrate, three dry films of 100 µm are successively laminated on it. This one is exposed with a first mask (I-line HR 66 mW at 1400 mJ cm^{-2}) and cured (6 min at 100 °C) by following standard photolithography processes. The second level is made from two successive laminations of 100 µm dry film sheets. Insolation is done using the second mask (I-line HR 66 mW, 900 mJ cm^{-2}) and the mold is finally cured (100 °C for 3 min). While performing the development bath overnight in SU8 developer, all the sliding elements progressively detach from the wafer substrate, as no adhesion promoter was used. Surface control is done using Scanning Electron Microscopy (MEB Hitachi S-4800). Finally, a perfluorodecyltrichlorosilane (FDTS) self-assembled monolayer is grafted onto the surface to prevent cell adhesion.

Cell culture and spheroid formation

A338 cell line[15] derived from a murine pancreatic tumor with an activating mutation of KRas oncogene ($KRas^{G12D}$) are culture in DMEM (Sigma-Aldrich) supplemented with 10% SVF (Sigma-Aldrich) and 1% penicillin–streptomycin (Sigma-Aldrich), at 37 °C and 5% CO_2. Spheroids are formed using

hanging droplet protocol. Typically, 15 μL droplets of a cell suspension (at approximatively 13 cells per μL) are dropped on a petri dish cover. To limit evaporation, 7 mL of PBS is placed on the other cover part. Spheroids of 100 μm in diameter are formed in two days. In this study, we transfected PIP-FUCCI into mouse pancreatic cancer cells (A338), and used HeLa transfected with 40 nm-GEMs (Genetically Encoded Multimeric nanoparticles) as in ref. 37.

Agarose confinement experiments

A 48-well plate is placed on ice. We prepare a low-melting agarose solution of 2% concentration and leave it at 37 °C to thermalize. 200 μL of medium containing the spheroid of 2/3 days old is then mixed with 200 μL of 2% low-melting agarose within the pipette. The 400 μL solution is placed on the 48-well plate on ice, to enable rapid polymerization of agarose at a final concentration of 1%. We find that this step is necessary to obtain a fully-embedded spheroid: if the polymerization occurs at room temperature, the spheroid sediments most of the time at the bottom of the well, and is not embedded in 3D.

C. elegans culture

We use the *C. elegans* strain N2 (wild type), which is kindly provided by Alfonso Pérez-Escudero. *C. elegans* populations are grown, maintained, and manipulated with standard techniques,[40] except that the NGM medium is replaced by M9 agar minimal medium (M9 minimal salts supplemented with 0.2% casamino acids, 0.4% glycerol, 2.0 μg mL^{-1} thiamine and 2.5 μg mL^{-1} cholesterol). Synchronized worms are grown on agar plates seeded with a lawn of the bacteria *Ochrobactrum vermis* at 22.5 °C. Adult worms are collected in an Eppendorf tube containing 1 mL of M9 liquid medium (M9 minimal salts) and then loaded inside the microfluidic chip with a syringe. A single worm is blocked inside the chamber of the chip, grown for 48 h, and fed with a unidirectional flow of a culture of *Ochrobactrum vermis* in M9 liquid, at a rate of 500 μL h^{-1}.

D. melanogaster culture and leg preparation

Leg discs from SqhKI[RFP]3B background *D. melanogaster* are dissected at a white pupal stage in Schneider's insect medium (Sigma-Aldrich, S9895) supplemented with 15% fetal calf serum and 0.5% penicillin–streptomycin, as well as 2 μg ml^{-1} 20-hydroxyecdysone (Sigma-Aldrich, H5142). Legs are then transferred into the microfluidic chamber. Leg discs are imaged with a LSM880 confocal microscope fitted with a Fast Airyscan module (Carl Zeiss) and equipped with a 40× Water NA-1.2 objective. Stacks of 150 images with a z-step of 1 μm are taken every 30 minutes, with a pixel size of 0.0171 μm per pixel. The laser power is set at 1%. Airyscan Z-stacks are processed through the ZEN software. Max projection images are computed and displayed in Fig. 2.

Loading spheroids and other organisms

First, the chip is filled with DMEM medium supplemented with 10% SVF and 1% penicillin–streptomycin. Then, the sliding element is inserted carefully in the device such that the cavities are aligned in front of the culture chambers. Spheroids and organisms are taken one by one using a tubing connected to a syringe. Their injection is done at the inlet localized on the side of the sliding element channel. Once a spheroid is in the channel, it will go through the sliding element and will enter the desired chamber for the high-throughput device, or the only chamber for the chemostat. This step is repeated until all the culture chambers are filled with spheroids for the high-throughput device. Then, the sliding element is moved so that each chamber is closed with a wall, or aligned with the slits/holes for feeding. The medium channel is connected to a syringe pump and a flow of 400 μL h^{-1} is applied.

Imaging conditions

A Zeiss observer microscope is used to perform the acquisition for several days. Biological samples were observed through a 63× objective. In bright-field, the exposure time was about 100 ms with 30% intensity. The environment is fixed at 37 °C with 5% CO2 during the experiment, thanks to a small incubator (Tokai-hit).

Experiment with the FUCCI cell cycle reporter

The PIP-FUCCI cell cycle reporter allows us to monitor cell cycle progression through the oscillatory expression of green and red fluorophores marking different phases of the cell cycle (Fig. 4a). We recorded 3 z-positions (every 5 μm) of both the GFP and RFP signals (150 ms at 15% intensity), on top of bright field, during the confined growth of spheroids, with one image every hour. We performed z-projections of the images and manually counted the green, red, and both green and red nuclei. We analyzed for each spheroid the total number of tagged cells as well as green alone cells (G1 cells), to extract the percentage of G1 cells and the percentage of cells in the S, G2, or M phases of the cell cycle (denoted S/G2/M). Statistics are presented in the caption of Fig. 4b.

Finite element simulations

The geometry of the microfluidic cages including the pressure sensor is simulated using Comsol multiphysics software with the solid mechanics module in stationary conditions. Once the geometry of the chamber is created, PDMS (polydimethylsiloxane) is set as a linear elastic material characterized by Young's modulus of 2 MPa, a Poisson coefficient of 0.49, and a density of 970 kg m^{-3}. Concerning boundary conditions, the pressure is applied on the chamber walls which are all free to deform. Finally, a mesh controlled by physics is applied to the structure and built with tetrahedron elements. For each applied pressure, the total displacement of the membrane is calculated. A

calibration curve describing the deformation as a function of pressure is used to calibrate all the experiments.

Surface tension measurement

During the buildup of growth-induced pressure, the aggregate morphs from a spheroid shape to a cuboid, where the curvature decreases from the radius of the spheroid to the radius of a cell, at a given mechanical pressure. Denoting P^0_{ext} the external pressure, P_{int} the internal pressure, R the radius of curvature, and γ the surface tension, the Laplace pressure equation can be written

$$P^0_{int} = P^0_{ext} + \frac{2\gamma}{R_0}$$

when the aggregate is a sphere, with R_0 its radius, and

$$P_{int} = P^0_{ext} + P_{mecha}(R = R_c) = P^0_{ext} + \frac{2\gamma}{R_c}$$

when the spheroid has morphed into a cuboid shape with curvature radius R_c which corresponds to the radius of a cell, and P_{mecha} $(R = R_c)$ the mechanical pressure at this time point. P_{mecha} $(R = R_c)$ is the pressure measured by the pressure sensor. At this surface, the curvature of the spheroid is ~ 0 μm^{-1}, the spheroid flattening on the sensor. Given that P_{mecha} $(R = R_c) \sim 300$ Pa, and $R_c \sim 10$ μm, one gets $\gamma \sim 1.5$ mN m^{-1} as a surface tension value.

Genetically-encoded multimeric nanoparticles imaging and diffusion analysis

Experiments are performed on a Leica DM IRB microscope with spinning-disk confocal (Yokogawa CSU-X1) with a nominal power of 100 mW and a Hamamatsu sCMOS camera (Orca flash 4.0 C13440) with a 63× objective. GEM nanoparticle movies are acquired by illumination with a 488 nm laser at full power. 30 images are acquired with no delay during 300 ms continual exposure at 100 Hz frame-rate. Particle tracking is achieved with the FIJI MOSAIC Suite to extract the trajectories of each particles. For each trajectory, we then compute the single particle time-averaged mean-square displacement, and fit the first 10 points (100 ms) with a linear model, to extract a single-particle diffusion coefficient at 100 ms, as in ref. 28. We then compute the mean and standard error of the mean for the thousands of trajectories collected.

Author contributions

ZBM, TiM, BA and MD designed the culture chambers. ZBM, TiM, BA, LM, RC and MD designed the sliding elements. FM, AL, LM and RC helped with microfabrication. TiM, CD, MDL, JGG and MD developed cell lines and performed spheroids experiments. ZBM, RDC, CG and MD performed the *C. elegans* experiments. ZBM, TaM and MS performed the *D. melanogaster* experiments. SL and MD developed the mathematical analysis. ZBM, TiM and MD wrote the manuscript. All authors brought corrections to the manuscript.

Conflicts of interest

There are no conflicts to declare.

Acknowledgements

The authors would like to thank B. Venzac for critical reading of the manuscript. This work was partly supported by the French Renatech network. MD would like to thank Inserm Plan Cancer (Press-Diag-Therapy and MechaEvo grants), INCa PLBIO and Cancéropôle Grand Sud-Ouest. This work is partly funded by the European Union (ERC, UnderPressure, grant agreement number 101039998). Views and opinions expressed are however those of the author(s) only and do not necessarily reflect those of the European Union or the European Research Council. Neither the European Union nor the granting authority can be held responsible for them.

References

1 G. Greco, M. Agostini, S. Barone and M. Cecchini, Embryo development in dynamic microfluidic systems, *Sens. Actuators, B*, 2017, **250**, 525–532, DOI: **10.1016/J.SNB.2017.04.186**.
2 M. C. Letizia, M. Cornaglia and R. Trouillon, *et al.*, Microfluidics-enabled phenotyping of a whole population of C. elegans worms over their embryonic and post-embryonic development at single-organism resolution, *Microsyst. Nanoeng.*, 2018, **4**(1), 1–11, DOI: **10.1038/s41378-018-0003-8**.
3 T. J. Levario, M. Zhan, B. Lim, S. Y. Shvartsman and H. Lu, Microfluidic trap array for massively parallel imaging of Drosophila embryos, *Nat. Protoc.*, 2013, **8**(4), 721–736, DOI: **10.1038/nprot.2013.034**.
4 X. Li, A. V. Valadez, P. Zuo and Z. Nie, Microfluidic 3D cell culture: potential application for tissue-based bioassays, *Bioanalysis*, 2012, **4**(12), 1509–1525, DOI: **10.4155/BIO.12.133**.
5 T. Mulholland, M. McAllister and S. Patek, *et al.*, Drug screening of biopsy-derived spheroids using a self-generated microfluidic concentration gradient, *Sci. Rep.*, 2018, **8**(1), 1–12, DOI: **10.1038/s41598-018-33055-0**.
6 W. Lim and S. Park, A Microfluidic Spheroid Culture Device with a Concentration Gradient Generator for High-Throughput Screening of Drug Efficacy, *Mol*, 2018, **23**(12), 3355, DOI: **10.3390/MOLECULES23123355**.
7 D. Huh, B. D. Matthews, A. Mammoto, M. Montoya-Zavala, H. Y. Hsin and D. E. Ingber, Reconstituting Organ-Level Lung Functions on a Chip, *Science*, 2010, **328**(5986), 1662–1668, DOI: **10.1126/science.1188302**.
8 M. D. Bourn, D. V. B. Batchelor and N. Ingram, *et al.*, High-throughput microfluidics for evaluating microbubble enhanced delivery of cancer therapeutics in spheroid cultures, *J. Controlled Release*, 2020, **326**, 13–24, DOI: **10.1016/J.JCONREL.2020.06.011**.

9 C. A. Paggi, B. Venzac, M. Karperien, J. C. H. Leijten and S. Le Gac, Monolithic microfluidic platform for exerting gradients of compression on cell-laden hydrogels, and application to a model of the articular cartilage, *Sens. Actuators, B*, 2020, **315**, 127917, DOI: **10.1016/j.snb.2020.127917**.

10 L. J. Holt, O. Hallatschek and M. Delarue, Mechano-chemostats to study the effects of compressive stress on yeast, *Methods Cell Biol.*, 2018, **147**, 215–231, DOI: **10.1016/bs.mcb.2018.06.010**.

11 H. T. Nia, H. Liu and G. Seano, *et al.*, Solid stress and elastic energy as measures of tumour mechanopathology, *Nat. Biomed. Eng.*, 2016, **1**(1), 0004, DOI: **10.1038/s41551-016-0004**.

12 P. P. Provenzano, C. Cuevas, A. E. Chang, V. K. Goel, D. D. Von Hoff and S. R. Hingorani, Enzymatic Targeting of the Stroma Ablates Physical Barriers to Treatment of Pancreatic Ductal Adenocarcinoma, *Cancer Cell*, 2012, **21**(3), 418–429, DOI: **10.1016/j.ccr.2012.01.007**.

13 K. Alessandri, B. R. Sarangi and V. V. Gurchenkov, *et al.*, Cellular capsules as a tool for multicellular spheroid production and for investigating the mechanics of tumor progression *in vitro*, *Proc. Natl. Acad. Sci. U. S. A.*, 2013, **110**(37), 14843–14848, DOI: **10.1073/pnas.1309482110**.

14 S. Nam, V. K. Gupta and H. Lee, *et al.*, Cell cycle progression in confining microenvironments is regulated by a growth-responsive TRPV4-PI3K/Akt-p27 ^{Kip1} signaling axis, *Sci. Adv.*, 2019, **5**(8), eaaw6171, DOI: **10.1126/sciadv.aaw6171**.

15 I. Rizzuti, P. Mascheroni and S. Arcucci, *et al.*, Mechanical Control of Cell Proliferation Increases Resistance to Chemotherapeutic Agents, *Phys. Rev. Lett.*, 2020, **125**(12), 128103, DOI: **10.1103/PhysRevLett.125.128103**.

16 G. Charras and A. S. Yap, Tensile Forces and Mechanotransduction at Cell–Cell Junctions, *Curr. Biol.*, 2018, **28**(8), 445–457, DOI: **10.1016/j.cub.2018.02.003**.

17 E. Faurobert, A.-P. Bouin and C. Albiges-Rizo, Microenvironment, tumor cell plasticity, and cancer, *Curr. Opin. Oncol.*, 2015, **27**(1), 64–70, DOI: **10.1097/CCO.0000000000000154**.

18 A. Athirasala, N. Hirsch and A. Buxboim, Nuclear mechanotransduction: sensing the force from within, *Curr. Opin. Cell Biol.*, 2017, **46**, 119–127, DOI: **10.1016/j.ceb.2017.04.004**.

19 M. Santoro, S.-E. Lamhamedi-Cherradi, B. A. Menegaz, J. A. Ludwig and A. G. Mikos, Flow perfusion effects on three-dimensional culture and drug sensitivity of Ewing sarcoma, *Proc. Natl. Acad. Sci.*, 2015, **112**(33), 10304–10309, DOI: **10.1073/pnas.1506684112**.

20 J. Xu, J. Mathur and E. Vessières, *et al.*, GPR68 Senses Flow and Is Essential for Vascular Physiology, *Cell*, 2018, **173**(3), 762–775.e16, DOI: **10.1016/j.cell.2018.03.076**.

21 J. Heo, F. Sachs, J. Wang and S. Z. Hua, Shear-induced volume decrease in MDCK cells, *Cell. Physiol. Biochem.*, 2012, **30**(2), 395–406, DOI: **10.1159/000339033**.

22 L. Aoun, P. Weiss, A. Laborde, B. Ducommun, V. Lobjois and C. Vieu, Microdevice arrays of high aspect ratio poly(dimethylsiloxane) pillars for the investigation of multicellular tumour spheroid mechanical properties, *Lab Chip*, 2014, **14**(13), 2344–2353, DOI: **10.1039/C4LC00197D**.

23 L. Aoun, S. Larnier and P. Weiss, *et al.*, Measure and characterization of the forces exerted by growing multicellular spheroids using microdevice arrays, *PLoS One*, 2019, **14**(5), e0217227, DOI: **10.1371/journal.pone.0217227**.

24 A. Groisman, C. Lobo and H. Cho, *et al.*, A microfluidic chemostat for experiments with bacterial and yeast cells, *Nat. Methods*, 2005, **2**(9), 685–689, DOI: **10.1038/nmeth784**.

25 B. Venzac, Y. Liu and I. Ferrante, *et al.*, Sliding walls: a new paradigm for fluidic actuation and protocol implementation in microfluidics, *Microsyst. Nanoeng.*, 2020, **6**(1), 1–10, DOI: **10.1038/s41378-019-0125-7**.

26 M. Basan, T. Risler, J.-F. Joanny, X. Sastre-Garau and J. Prost, Homeostatic competition drives tumor growth and metastasis nucleation, *HFSP J.*, 2009, **3**(4), 265–272, DOI: **10.2976/1.3086732**.

27 C. M. Denais, R. M. Gilbert and P. Isermann, *et al.*, Nuclear envelope rupture and repair during cancer cell migration, *Science*, 2016, **352**(6283), 353–358, DOI: **10.1126/SCIENCE.AAD7297/SUPPL_FILE/PAPV2.PDF**.

28 B. Alric, C. Formosa-Dague and E. Dague, *et al.*, Macromolecular crowding limits growth under pressure, *Nat. Phys.*, 2022, **18**, 411–416, DOI: **10.1038/s41567-022-01506-1**.

29 G. Helmlinger, P. A. Netti, H. C. Lichtenbeld, R. J. Melder and R. K. Jain, Solid stress inhibits the growth of multicellular tumor spheroids, *Nat. Biotechnol.*, 1997, **15**(8), 778–783, DOI: **10.1038/nbt0897-778**.

30 M. E. Dolega, M. Delarue, F. Ingremeau, J. Prost, A. Delon and G. Cappello, Cell-like pressure sensors reveal increase of mechanical stress towards the core of multicellular spheroids under compression, *Nat. Commun.*, 2017, **8**, 14056, DOI: **10.1038/ncomms14056**.

31 W. Lee, N. Kalashnikov and S. Mok, *et al.*, Dispersible hydrogel force sensors reveal patterns of solid mechanical stress in multicellular spheroid cultures, *Nat. Commun.*, 2019, **10**(1), 144, DOI: **10.1038/s41467-018-07967-4**.

32 M. Gupta, L. Kocgozlu, B. R. Sarangi, F. Margadant, M. Ashraf and B. Ladoux, Micropillar substrates: A tool for studying cell mechanobiology, *Methods Cell Biol.*, 2015, **125**, 289–308, DOI: **10.1016/BS.MCB.2014.10.009**.

33 K. Guevorkian, M. J. Colbert, M. Durth, S. Dufour and F. Brochard-Wyart, Aspiration of biological viscoelastic drops, *Phys. Rev. Lett.*, 2010, **104**(21), 218101, DOI: **10.1103/PHYSREVLETT.104.218101/FIGURES/4/MEDIUM**.

34 S. Nam, V. K. Gupta and H.-P. Lee, *et al.*, Cell cycle progression in confining microenvironments is regulated by a growth-responsive TRPV4-PI3K/Akt-p27Kip1 signaling axis, *Sci. Adv.*, 2019, **5**(8), eaaw6171, DOI: **10.1126/sciadv.aaw6171**.

35 G. Cheng, J. Tse, R. K. Jain and L. L. Munn, Micro-environmental mechanical stress controls tumor spheroid size and morphology by suppressing proliferation and inducing apoptosis in cancer cells, *PLoS One*, 2009, **4**(2), e4632, DOI: **10.1371/journal.pone.0004632**.

36 R. J. Ellis, Macromolecular crowding: An important but neglected aspect of the intracellular environment, *Curr.*

Opin. Struct. Biol., 2001, **11**(1), 114–119, DOI: **10.1016/S0959-440X(00)00172-X**.

37 M. Delarue, G. P. Brittingham and S. Pfeffer, *et al.*, mTORC1 Controls Phase Separation and the Biophysical Properties of the Cytoplasm by Tuning Crowding, *Cell*, 2018, **174**, 1–12, DOI: **10.1016/j.cell.2018.05.042**.

38 A. Proag, B. Monier and M. Suzanne, Physical and functional cell-matrix uncoupling in a developing tissue under tension, *Development*, 2019, **146**(11), dev172577, DOI: **10.1242/dev.172577**.

39 P. Mandaron, C. Glillermet and P. Sengel, *In Vitro* Development of Drosophila Imaginal Discs: Hormonal Control and Mechanism of Evagination, *Integr. Comp. Biol.*, 1977, **17**(3), 661–670, DOI: **10.1093/ICB/17.3.661**.

40 T. Stiernagle, Maintenance of C. elegans, *WormBook*, 2006, pp. 1–11, Published online, DOI: **10.1895/WORMBOOK.1.101.1**.